

Article

Phonon Blockade in Parametrically Pumped Acoustic Cavity at Finite Temperature

Zhenglu Duan , Yongkang Shao, Yi Ren and Biao Huang

College of Physics, Communication and Electrons, Jiangxi Normal University, Nanchang 330022, China

* Correspondence: duanzhenglu@jxnu.edu.cn

Abstract: In this study, we investigated the phonon blockade effect in a parametrically driven and dissipative acoustic cavity at finite temperature. With the approximated analytical results based on the steady-state density-matrix master equation, we found that a quantum-interference-induced phonon blockade exists at finite temperature. We found a crossover between the quantum and thermal regimes on the curve of the second-order correlation function of the acoustic mode as the temperature increases. This phenomenon implies an asymmetry about the quantum and classic regimes. We also numerically simulated the single-phonon emission using the Monte Carlo wave function method. The results showed that a wide and deep dip around the zero time delay exists on the curve of the time-delayed second-order correlation function, which implies the possibility of observing a strong phonon blockade with pulse driving. Our study outlines a potential candidate for a efficient single-phonon source and applications in quantum information and phononic quantum networks.

Keywords: phonon blockade; acoustic cavity; finite temperature

1. Introduction

Quantum state transfer and storage are important in quantum information processing. Currently, the photon is commonly used as the quantum carrier for transferring and storing quantum information, which is high speed and robust against environmental noise. Recently, phonons, as a new candidate for carrying quantum information, have attracted the attention of researchers [1–5]. Phonons are the vibrational modes of mechanical oscillators; they have the ability to maintain a long coherence time, low traveling velocity, and long wavelength; and they interact with a wide range of other quantum systems, such as electric, magnetic, and optical systems. In all quantum phononic networks, a single phonon source is an important element. Phonon blockade is the phenomenon in which the phonons in acoustic systems exhibit single-time antibunching behavior ($1 > g^{(2)}(0)$), which was first investigated in Ref. [6]. Therefore, phonon blockade was proposed to prepare single-phonon sources [7,8] and other potential single-phonon devices [2,3].

Phonon blockade can be achieved with two main methods: conventional phonon blockade (CPNB) [6,9–12], resulting from the strong-nonlinearity-induced nonuniform energy ladders, and unconventional phonon blockade (UCPNB) [13–21], resulting from the interference between the different quantum transition paths of phonons. The mean phonon number (the brightness of a phonon source) produced by CPNB is relatively large; however, its antibunching (purity) is limited. Phonons produced by UCPNB exhibit higher purity, but the mean phonon number is lower. In general, CPNB operates in a strong nonlinear regime, whereas only weak nonlinearity is required for UCPNB. Owing to the weak intrinsic nonlinearity of a mechanical resonator, researchers have studied the CPNB mainly in composite quantum systems, such as a resonator two-level system [11,12] and an optomechanical system [22–24]. More recently, nonreciprocal phonon blockade and two phonon blockade have also been observed in a spinning acoustic ring cavity coupled to a two-level system [25] and optomechanical system [26], respectively. Here, we stress



Citation: Duan, Z.; Shao, Y.; Ren, Y.; Huang, B. Phonon Blockade in Parametrically Pumped Acoustic Cavity at Finite Temperature. *Symmetry* **2023**, *15*, 245. <https://doi.org/10.3390/sym15010245>

Academic Editor: Wiesław Leonski

Received: 7 December 2022

Revised: 8 January 2023

Accepted: 13 January 2023

Published: 16 January 2023



Copyright: © 2023 by the authors. Licensee MDPI, Basel, Switzerland. This article is an open access article distributed under the terms and conditions of the Creative Commons Attribution (CC BY) license (<https://creativecommons.org/licenses/by/4.0/>).

that for a true good single phonon, both $g^{(2)}(0) < 1$ and $g^{(k)}(0) < 1$, ($k = 3, 4, \dots$) are required [27].

Different from that of photons, the frequency of phonons is relatively low; therefore, the thermal noise at finite temperature, e.g., at room temperature, can easily destroy the quantum behavior of the acoustic field. To observe the quantum behavior of a phonon system, the mechanical resonator must be cooled to a very low temperature. With the rapid development in micro-/nanomechanical manufacturing technology [28–31], a mechanical resonator can be cooled near to its quantum ground state [32]. However, the thermal noise in mechanical resonators cannot be completely eliminated, and the phonon blockade is sensitive to thermal noise. Hence, the realization of phonon blockade with thermal noise and the preparation of single-phonon source with high quality at finite temperature remains challenging. Additionally, few studies have been conducted with the Monte Carlo wave function method to reveal phonon blockade [33].

Motivated by the above-mentioned studies, we examined phonon blockade in a quantum acoustic system consisting of a parametrically driven nanomechanical resonator at finite temperature, where its spring constant is periodically modulated. To periodically modulate the spring constant of the nanomechanical resonator, we placed an electrode below the nanomechanical resonator and applied a time-varying voltage with a frequency twice that of the nanomechanical resonator. The gradient of the electrostatic force from the electrode can modify the spring constant and realize a parametric pump [34–37]. Compared with the other phonon blockade schemes, we theoretically show the realization of UCPNB without the intrinsic mechanical nonlinearity or an auxiliary nonlinear system [14–21]. Furthermore, we implemented the Monte Carlo wave function method to illustrate the phononic statistics at finite temperature. Due to the lack of auxiliary system, no oscillation occurs in the curve of the time-delayed second-order correlation function of the acoustic field, which is helpful for generating a single phonon with pulse excitation.

The remainder of this paper is organized as follows: In Section 2, we describe the model and present the analytical results based on the density matrix master equation. In Section 3, we discuss the quantum statistics of the phonon mode at zero and finite temperature. In Section 4, we illustrate the phonon antibunching effect with Monte Carlo simulation. Finally, we conclude this paper in Section 5.

2. Model and Analysis

The model under consideration is a mechanical oscillator driven by an external force and a parametric pump [37]. The Hamiltonian system is given by

$$H = \frac{\hat{P}^2}{2m} + \frac{1}{2}m\omega_m^2(1 + g \cos(2\omega_m t + 2\theta))\hat{X}^2 + F \cos(\omega_d t)\hat{X},$$

where \hat{X} and \hat{P} are the displacement and momentum of the mechanical oscillator, respectively, with effective mass m , resonance frequency ω_m , and damp rate γ ; F is the amplitude of the external driving force with driving frequency ω_d ; g is the modulation amplitude. The parametric pump frequency is $2\omega_m$ with a relative phase angle θ . To more conveniently describe the quantum feature of the mechanical oscillator, we introduce phonon annihilation ($\hat{a} = (\hat{X} + i\hat{P})/\sqrt{2}$) and creation ($\hat{a}^\dagger = (\hat{X} - i\hat{P})/\sqrt{2}$) operators, which satisfy the commutators $[\hat{a}, \hat{a}^\dagger] = 1$. After rotating at the driving frequency ω_d , the Hamiltonian system becomes ($\hbar = 1$):

$$H = \Delta_0 \hat{a}^\dagger \hat{a} + i\chi \left(e^{2i\theta} \hat{a}^2 - e^{-2i\theta} \hat{a}^{2\dagger} \right) + F \left(\hat{a}^\dagger + \hat{a} \right), \quad (1)$$

where $\Delta_0 = \omega_m - \omega_d$ represents the detuning between the resonance frequency of the mechanical oscillator and driving force; $\chi = \omega_m g/2$ is the effective parametric pump strength. The Hamiltonian (Equation (1)) is similar to the optical counterpart where a driven-dissipation optical cavity is filled with a $\chi^{(2)}$ medium [33,38].

The dynamics of our system with the inclusion of dissipation are governed by the master equation for the density matrix:

$$\frac{d\hat{\rho}}{dt} = L\hat{\rho}, \quad (2)$$

where superoperator L is defined as:

$$L\hat{\rho} = -i[H, \hat{\rho}] + \frac{\kappa}{2} \left[(1 + \bar{n})D[\hat{a}]\hat{\rho} + \bar{n}D[\hat{a}^\dagger]\hat{\rho} \right]$$

with Lindblad operator $D[\hat{A}]\hat{\rho} = 2\hat{A}\hat{\rho}\hat{A}^\dagger - \hat{A}^\dagger\hat{A}\hat{\rho} - \hat{\rho}\hat{A}^\dagger\hat{A}$. κ is the decay rate of the acoustic cavity. The thermal phonon number is $\bar{n} = (\exp(T_0/T) - 1)^{-1}$ at temperature T , where $T_0 = \hbar\omega_m/K_B$ is the characteristic temperature of the quantum acoustic system with the Boltzmann constant K_B .

Our main focus was investigating quantum statistic properties of the acoustic mode of a mechanical oscillator. In quantum optics, the second-order correlation function $g_{t \rightarrow \infty}^{(2)}(\tau) = \langle \hat{a}^\dagger(t)\hat{a}^\dagger(t+\tau)\hat{a}(t+\tau)\hat{a}(t) \rangle / \langle \hat{a}^\dagger(t)\hat{a}(t) \rangle^2$ is a standard measure of quantum statistics of bosons, such as photons and phonons. $g^{(2)}(0) > 1$ ($g^{(2)}(0) < 1$) is a super-Poissonian (sub-Poissonian) distribution of bosons [27,38,39]. Therefore, in the following, we study the phonon blockade property via evaluating the equal-time second-order correlation function of phonons:

$$g^{(2)}(0) = \frac{\text{Tr}(\hat{a}^{\dagger 2}\hat{a}^2\hat{\rho}_{ss})}{\text{Tr}(\hat{a}^\dagger\hat{a}\hat{\rho}_{ss})^2} \quad (3)$$

where ρ_{ss} is the steady-state density matrix corresponding to $d\hat{\rho}/dt = 0$ in Equation (2). In the calculation, we express the density matrix $\hat{\rho} = \sum_{m,n=0} \rho_{mn}|m\rangle\langle n|$ on the basis of phonon number state $|m\rangle$, which is truncated as a finite Hilbert space of the system with the assumption of a weak driving (pump) limit, i.e., $F, \chi \ll \kappa$.

We first present the approximate analytical expression for the steady-state density matrix using the perturbation method (Please see Appendix A). In the weak driving and low temperature limits, low mechanical excitations result in $\rho_{00} \gg \rho_{11} \gg \rho_{22} \gg \rho_{33}$. After tedious calculation using perturbation theory, we obtain the expression for the equal-time second-order correlation function $g^{(2)}(0)$ at finite temperature:

$$g^{(2)}(0) \approx \frac{2\rho_{22} + 6\rho_{33}}{(\rho_{11} + 2\rho_{22} + 3\rho_{33})^2}, \quad (4)$$

where the density matrix elements are given by:

$$\rho_{11} = \frac{\bar{n}|\Delta|^2 + F^2}{(1 + 2\bar{n})|\Delta|^2 + 2F^2} \quad (5)$$

$$\begin{aligned} \rho_{22} = & \left(1 - \frac{6F^2}{|\Delta|^2}\right)\bar{n}^2 + \frac{|F^2 - \Delta\chi e^{i\theta}|^2}{|\Delta|^4}\bar{n} \\ & + \frac{\chi^2|\Delta|^2 - 3F^4 + 2F^2|\Delta|^2}{|\Delta|^4}\bar{n} + \frac{3\chi^2|\Delta|^2 - F^4}{|\Delta|^6}F^2 \\ & + \frac{(2E^2 + |\Delta|^2)|F^2 - \Delta\chi e^{i\theta}|^2}{2|\Delta|^6} \end{aligned} \quad (6)$$

$$\rho_{33} = \frac{3F^2}{|\Delta|^2}\bar{n}^2 + \frac{3|F^2 - \Delta\chi e^{i\theta}|^2}{2|\Delta|^4}\bar{n} + \frac{|F^2 - 3\Delta\chi e^{i\theta}|^2 F^2}{6|\Delta|^6} \quad (7)$$

with effective detuning $\Delta = \Delta_0 - i\kappa/2$.

3. Quantum Statistics of Phonon Mode

In this section, we describe the phonon blockade effect of a parametrically pumped mechanical oscillator and the influence of thermal noise on phonon blockade behavior.

3.1. Phonon Blockade Effect at Zero Temperature

At zero temperature, Equation (4) reduces to:

$$g^{(2)}(0) = \frac{(|\Delta|^2 + 2F^2)^2}{F^4|\Delta|^6} \left(2F^2 + |\Delta|^2 \right) \left| F^2 - \Delta\chi e^{i\theta} \right|^2 + \frac{(|\Delta|^2 + 2F^2)^2}{F^2|\Delta|^6} \left(6\chi^2|\Delta|^2 - 2F^4 + \left| F^2 - 3\Delta\chi e^{i\theta} \right|^2 \right). \quad (8)$$

Equation (8) shows that if $F^2 = \Delta\chi e^{i\theta}$, the second-order correlation function takes its minimal value $g_{\min}^2(0) = 8F^2 / (\Delta_0^2 + \kappa^2/4)$, which is far below 1 in the weak driving limit ($F \ll \kappa$). Thus, the condition for optimal blockade of phonon mode is

$$\theta = \tan^{-1} \left(\frac{\kappa}{2\Delta_0} \right) \quad (9)$$

$$\chi = F^2 / \sqrt{\Delta_0^2 + \kappa^2/4} \quad (10)$$

When the system operates under the optimal condition (Equation (10)), the mean phonon number $\langle N \rangle \equiv \text{Tr}(\hat{a}^\dagger \hat{a} \hat{\rho}_{ss}) \approx F^2 / (\Delta_0^2 + \kappa^2/4)$ and the minimal second-order correlation function $g_{\min}^2(0) = 8\langle N \rangle$, which imply that we cannot simultaneously enhance the blockade effect and increase the mean phonon number by decreasing the driving strength. This is because the physical mechanism of the phonon blockade in this study is the destructive interference between two quantum transition paths, $|0\rangle \rightarrow |2\rangle$ and $|0\rangle \rightarrow |1\rangle \rightarrow |2\rangle$, as shown in Figure 1b.

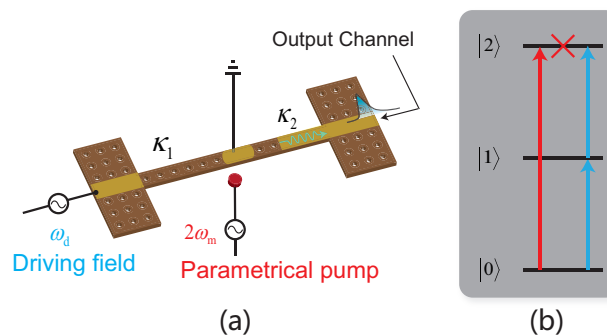


Figure 1. (a) Schematic diagram of nanobeam driven by coherent acoustic field and parametric pump. (b) Energy level structure of the quantum acoustic system.

To further illustrate the quantum statistics of phonon mode, we plot the equal-time second-order correlation function $g^{(2)}(0)$ as functions of F , χ and Δ_0 in Figure 2a,b by numerically integrating the master Equation (Equation (2)). We show that the phonon blockade effect exists in a large parameter space, which is indicated by the blue region. We also label the optimal parameter condition given by Equations (9) and (10) with green dashed curves. The strongest blockade effect occurs along the optimal-condition curves, as shown in Figure 2a,b. To clearly observe the behavior of the optimal second-order correlation function, we plot the second-order correlation function with the optimal condition in Figure 2c,d. The optimal second-order correlation function decreases with increasing detuning when the optimal blockade conditions (Equations (9) and (10)) hold. Additionally,

high-order correlation functions, e.g., $g^{(3)}(0)$ and $g^{(4)}(0)$, are presented in Figure 2c,d with the optimal condition (Equations (9) and (10)) holding. $\{g^{(3)}(0), g^{(4)}(0)\} > 1 > g^{(2)}(0)$, which is a typical feature of UCPNB. This conclusion is consistent with the previous discussion based on quantum interference. The phonon blockade studied here comes from a special squeezed state of the phonon field. Similar effects were demonstrated in its photonic counterpart [27,38].

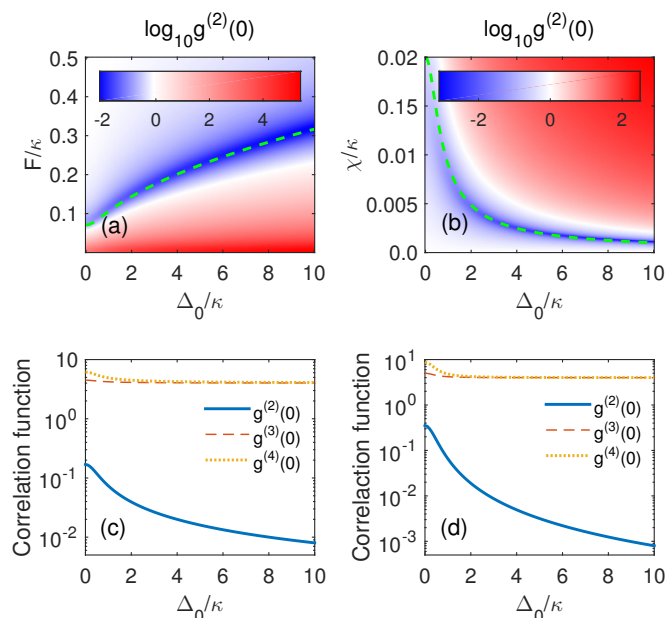


Figure 2. (a) $\text{Log}_{10}(g^{(2)}(0))$ as functions of F and Δ_0 with fixed $\chi = 0.01\kappa$. (b) $\text{Log}_{10}g^{(2)}(0)$ as functions of χ and Δ_0 with fixed $F = 0.1\kappa$. Green dashed lines in (a,b) are the curves satisfy the optimal conditions (Equations (9) and (10)). (c,d) Plots of correlation functions determined by the optimal conditions (Equations (9) and (10)) with $\chi = 0.01\kappa$ and $F = 0.1\kappa$, respectively.

3.2. Phonon Blockade Effect at Finite Temperature

We then studied the influence of thermal noise at finite temperature on the quantum statistics of phonon mod. Figure 3a,b plots the second-order correlation function as functions of the detuning Δ and driving strength F at temperatures $0.05T_0$ and $0.1T_0$, respectively. Compared with the case of zero temperature (as shown in Figure 2a), the optimal blockade feature is almost unchanged for $T = 0.05T_0$ (as shown in Figure 3a), while the blockade effect exhibits obvious deterioration for $T = 0.1T_0$ (as shown in Figure 3b). The blockade of phonon mode can only survive at relatively low temperature.

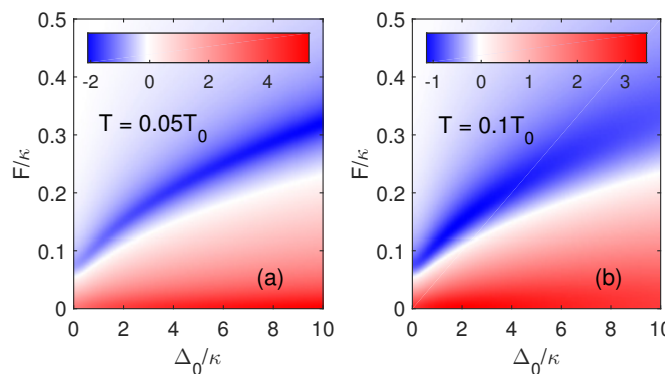


Figure 3. $\text{Log}_{10}(g^{(2)}(0))$ as functions of F and Δ_0 for two different temperatures: (a) $T = 0.05T_0$ and (b) $T = 0.1T_0$. Other parameters are: $\chi = 0.01\kappa$ and $\theta = -\tan^{-1}(\frac{\kappa}{2\Delta_0})$.

To determine the critical temperatures, we plot the second-order correlation function as a function of the temperature of the bath, with other parameters satisfying the optimal conditions (Equations (9) and (10)) in Figure 4a. As we increase the temperature T , $g^{(2)}(0)$ almost remains a constant value far less than 1 for the temperatures below a threshold value T_{c1} ; then, it experiences a sharp rise for temperatures between T_{c1} and T_{c2} ; finally, it tends to constant (2) for $T > T_{c2}$. Based on these findings, we can divide the second-order correlation function into three regimes in terms of bath temperature: (i) low-temperature regime ($T < T_{c1}$); (ii) crossover regime ($T_{c1} < T < T_{c2}$); and (iii) high-temperature regime ($T > T_{c2}$). To further clarify the relationship between $g^{(2)}(0)$ and temperature T , we substitute the optimal conditions (Equations (9) and (10)) into the expression of the second-order correlation function (Equation (4)) and obtain an approximate expression

$$g^{(2)}(0) \approx 2 \frac{4F^6/|\Delta|^6 + 2F^2\bar{n}/|\Delta|^2 + \bar{n}^2}{(\bar{n} + F^2/|\Delta|^2)^2} \tag{11}$$

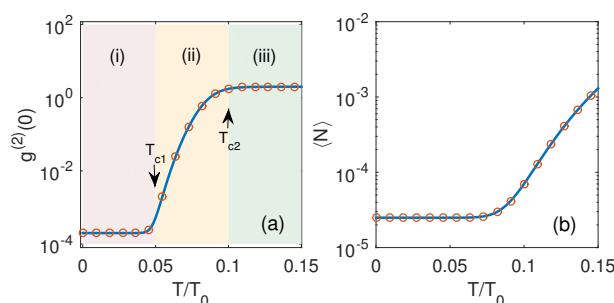


Figure 4. (a) Second-order correlation function $g^{(2)}(0)$ and (b) mean phonon number $\langle N \rangle$ as a function of bath temperature T with acoustic cavity detuning $\Delta_0 = 10\kappa$ and driving strength $F = 0.05\kappa$. The other parameters are determined by the optimal conditions (Equations (9) and (10)). The symbol “o” represents the analytical results (Equations (11) and (12)) with the same parameters.

By examining Equation (11), we can see that at low temperature, the first term in the numerator (the quantum coherence term) is dominant, and the second-order correlation function $g^{(2)}(0)$ is small. With increasing environmental temperature, the thermal noise becomes important. When the environmental temperature reaches a critical value T_{c1} , the first term in numerator of the right-hand side of Equation (11) is equal to the second term and larger than the third term, that is, $4F^6/|\Delta|^6 \approx 2\bar{n}F^2/|\Delta|^2 \gg \bar{n}^2$. We can obtain $\bar{n}_{c1} \approx 2F^4/|\Delta|^4$ and the corresponding critical temperature $T_{c1} \approx T_0/\ln(|\Delta|^4/2F^4)$. When $T > T_{c1}$, the contribution to the correlation function by the quantum coherence term less than that by the thermal term. When the environmental temperature continuously rises and reaches T_{c2} , the third term in the numerator of the expression of $g^{(2)}(0)$ is equal to the second term and much larger than the first term, i.e., $\bar{n}^2 \approx 2\bar{n}F^2/|\Delta|^2 \gg 4F^6/|\Delta|^6$. We find $\bar{n}_{c2} \approx 2F^2/|\Delta|^2$ and the corresponding critical temperature $T_{c2} \approx T_0/\ln(|\Delta|^2/2F^2)$. When $T > T_{c2}$, the thermal noise term is dominant in the system, which is denoted as $g^{(2)}(0) \rightarrow 2$. The underlying physics is that the large thermal noise can destroy the quantum coherence of the quantum acoustic system. Therefore, we need a relatively low temperature to experimentally observe the optimal phonon blockade. The asymmetry of the autocorrelation about the environmental temperature comes from the non-equivalence in the quantum and classic regimes. To evaluate the critical temperature, we set $F = 0.05\kappa$ and $\Delta_0 = 10\kappa$, and we obtain $T_{c1} = 0.05T_0$ and $T_{c2} = 0.1T_0$. The analytical results are consistent with the numerical values, as shown in Figure 4a.

In addition, we present the mean phonon number versus the bath temperature under the optimal condition. Figure 4b shows that as the temperature increases, the mean phonon number is first a constant value and then exponentially increases when the bath temperature is larger than a threshold value. To explain this phenomenon, we provide the analytical ex-

pression of the mean phonon number under the optimal conditions (Equations (9) and (10)) as follows:

$$\langle N \rangle \approx \rho_{11} \approx F^2/|\Delta|^2 + \bar{n}. \tag{12}$$

From Equation (12), we see that for the low-temperature regime, $F^2/|\Delta|^2 \gg \bar{n}$, the term of thermal noise can be neglected, and the mean phonon number $\langle N \rangle$ is a constant $F^2/|\Delta|^2$. The threshold value can be defined as that at which the quantum coherence term is equal to the noise term, i.e., $F^2/|\Delta|^2 \sim \bar{n}$. Then, the threshold temperature can be obtained as $T \approx 0.09T_0$ for $F = 0.05\kappa$ and $\Delta_0 = 10\kappa$. This value agrees well with the numerical result, indicated by a vertical dashed curve in Figure 4. At high temperature, the thermal noise dominates; hence, $\langle N \rangle \approx \bar{n}$, which leads to an exponential increase in the mean phonon number.

We then investigated the effect of the driving strength on the second-order correlation function and the mean phonon number at different bath temperatures under optimal conditions (Equations (9) and (10)). Figure 5 shows that at zero temperature, the second-order correlation function of the phonon mode increases with increasing driving strength, whereas at finite temperature, the second-order correlation function of the phonon mode first decreases and then increases as the driving strength increases. This can be explained as follows: for $T = 0$, Equation (11) is reduced into $g^{(2)}(0) \approx 8F^2/|\Delta|^2$, which means the second-order correlation function is quadratically dependent on the driving strength. For finite temperatures, when $F \rightarrow 0$, the quantum coherence term approaches zero, and the thermal noise dominates the acoustic system, which leads to $g^{(2)}(0) \rightarrow 2$. When the driving strength increases, the quantum coherence rather than the thermal noise gradually dominates the second-order correlation function; hence, the second-order correlation function decreases from 2. If the driving strength becomes strong enough, higher phonon number states are dramatically populated, resulting in the second-order correlation function increasing again and then approaching 1, which means the acoustic system reaches the coherent state. The result indicates that a proper driving strength, rather than an infinitesimal one, can lead to optimal phonon blockade at finite temperature. We also studied the effect of driving strength on the mean phonon number. Figure 5b shows a monotonically increasing mean phonon number with increasing driving strength for all bath temperatures. This can be explained from the expression of the mean phonon number $\langle N \rangle \approx (|\Delta|^2/(\bar{n}|\Delta|^2 + F^2) + 2)^{-1}$.

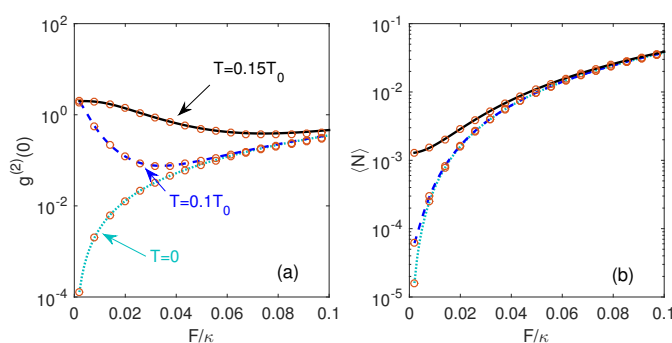


Figure 5. (a) Second-order correlation function $g^{(2)}(0)$ and (b) mean phonon number $\langle N \rangle$ as a function of driving strength F with bath temperature $T = 0$ (dotted curves), $T = 0.1T_0$ (dashed curves), and $T = 0.15T_0$ (solid curves). Cavity detuning $\Delta_0 = 0$ and other parameters are determined by optimal conditions (Equations (9) and (10)). The symbol “o” represents the analytical results (Equations (11) and (12)) with the same parameters.

4. Quantum Statistics of Phonons with Monte Carlo Simulation

To further study the quantum properties of the phonon mode, we implemented the Monte Carlo wave-function method to simulate the evolution of the quantum acoustic system and count the photons at the output port [33,40]. This method is analogous to the phonon Hanbury–Brown–Twiss (HBT) experimental procedure. We obtained the

correlation information of the emitted phonons from sufficiently long stochastic trajectories. In the following, we describe the procedure of the Monte Carlo wave-function method for simulating the stochastic phonon emission from an acoustic cavity.

Assuming a phonon count at time t , we then cumulate the emitted phonons from the acoustic cavity $N(t, t + \tau)$ in an interval $\Delta\tau$. When choosing the interval $\Delta\tau$, we must consider the balance between the resolution and statistical fluctuation. By averaging all $N(t, t_j)$ over all t , $\bar{N}(t, t_j) = \sum_t N(t, t_j) / N_{total}$, with the total emitted phonon number N_{total} within the total counting time duration T . For sufficiently large samples, if we detect a phonon at time t , then the average value is dependent on the conditional probability of finding the second phonon at time $t + \tau$. Finally, the second-order correlation function with the time delay τ is presented as follows:

$$g^2(\tau) = \frac{\bar{N}(t, t + \tau)}{\bar{N}(t)}, \quad (13)$$

where $\bar{N}(t) = N_{total}\Delta\tau/T$ is the mean emitted phonon number in an interval $\Delta\tau$ when the system is in the steady state.

In the numerical experiment, we set the detuning $\Delta_0 = 0$, relative phase $\theta = \pi/2$, resonance frequency of the acoustic cavity $\omega_m = 5$ GHz, effective parametric pump strength $\chi = 50$ kHz, driving strength $F = 500$ kHz, and leak rate of acoustic cavity to the input and output channel to $\kappa_1 \simeq 10$ MHz and $\kappa_2 \simeq 0.1$ MHz, respectively. These parameters are typical values feasible in experiments. The total decay was $\kappa = \kappa_1 + \kappa_2 \simeq \kappa_1$. The other system parameters were determined by fulfilling the optimal conditions (Equations (9) and (10)).

Figure 6a shows a typical Monte Carlo trajectory of the mean phonon number in an acoustic cavity at bath temperature $T = 0.15T_0 = 5.4$ mK. We can observe the random jumps of phonons induced by the thermal bath and the leakage of the phonon cavity in the time domain. The histograms in Figure 6b–d are the statistical results of $g^{(2)}(\tau)$ for different bath temperatures. The total accumulated time for each single trajectory was 0.25 s in the simulation. Figure 6b shows a deep dip at $\tau = 0$, where strong phonon antibunching ($g^{(2)}(0) < g^{(2)}(\tau)$) appears within delay $\tau < 0.5$ μ s when the bath temperature is zero. The minimal value of the time-delayed second-order correlation function $g_{min}^{(2)}(\tau) \simeq 0.08$, located at zero time delay $\tau = 0$. For a larger delay, the correlation function $g^{(2)}(\tau)$ tends exponentially to unitary. Given the phonon life time of $\sim\kappa_1^{-1} = 0.1$ μ s, we observe strong phonon antibunching in the pulse excitation situation with a sufficiently large pulse width in the time domain. Additionally, we count the total leaked phonon number $\sim 24,700$ in 0.25 s from the acoustic cavity, corresponding to an average phonon number 99,000 per second. Figure 6c,d show the time-delayed second-order correlation function with bath temperature $0.15T_0$ and $0.5T_0$. The second-order correlation function with zero time delay increases with increasing bath temperature and finally reaches two.

To verify the correctness of the results from Monte Carlo wave function method, we calculated the time-dependent second-order correlation function using quantum regression theorem [41]

$$g^{(2)}(\tau) = \frac{\text{Tr} \{ \hat{a}^\dagger \hat{a} e^{\hat{L}\tau} [\hat{a} \hat{\rho}_{ss} \hat{a}^\dagger] \}}{\text{Tr} (\hat{a}^\dagger \hat{a} \hat{\rho}_{ss})^2}. \quad (14)$$

The pink solid curve in Figure 6b–d is the result obtained based on Equation (14), which well reproduces the Monte Carlo simulation results. Therefore, we concluded that our numerical results based on the Monte Carlo wave function method are reliable.

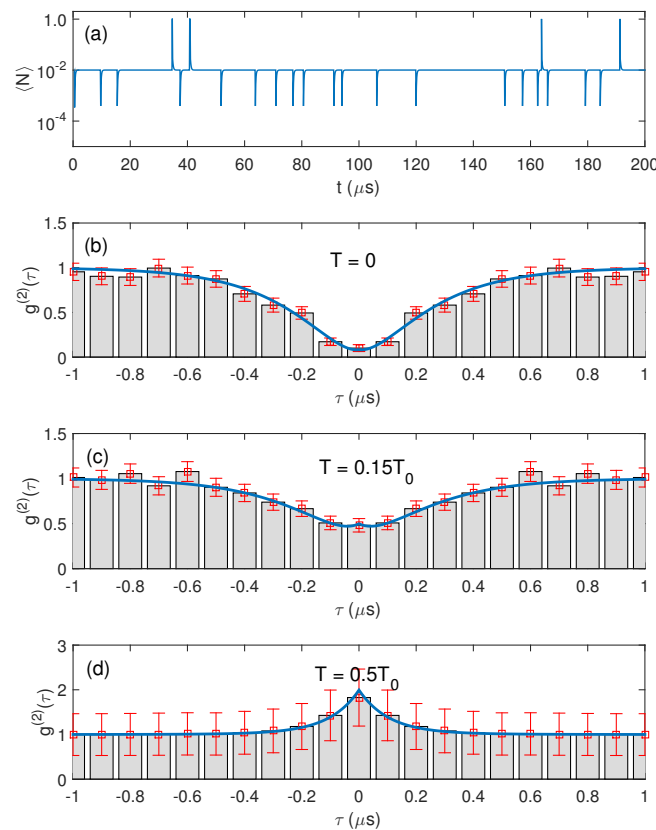


Figure 6. (a) Example of single Monte Carlo trajectory of phonon number in acoustic cavity with bath temperature $T = 0.15T_0$. (b–d) Time-delayed second-order correlation function $g^{(2)}(\tau)$ extracted from numerical experiment (histograms) and evaluated based on quantum regression theorem (Equation (14)) (thick blue solid curves) with different bath temperatures. Driving strength $F = 0.05\kappa$. Other parameters were determined by optimal conditions (Equation (9) and (10)).

5. Conclusions

We studied the phonon blockade phenomena in a parametrically pumped mechanical oscillator at zero and finite temperatures. We first analytically presented the optimal condition for strong phonon blockade based on the density-matrix master equation. When the acoustic system operates under the optimal condition, the second-order correlation function experiences a transition from sub-Poissonian to super-Poissonian phonon-number statistics as the bath temperature increases. Additionally, the second-order correlation function monotonically increases with increasing driving strength for zero temperature, whereas it first decreases and then increases for finite temperature. This means that a suitable driving strength, rather than an infinitesimal one, is suitable for obtaining a minimal second-order correlation function at finite temperature. Finally, we presented our numerical simulations of the time-delayed second-order correlation functions using the Monte Carlo wave-function method. The result showed that a wide and deep dip occurs on the second-order correlation function curve around the zero time delay when the system resonantly operates, i.e., $\Delta_0 = 0$. It suggests the possibility of observing strong phonon blockade in the pulse excitation regime. We presented an applicable scheme to generate single phonons at finite temperature, which is helpful for constructing a feasible single phonon source in experiments. Such single phonon device can be used in the field of quantum information and precise measurement based on quantum phononics. Finally, we should stress that, limited by the physical mechanism of UCPNB, the mean phonon number of our scheme is less than that of CPNB. As such, the proposed scheme may not be applicable in scenarios requiring high single phonon generation efficiency from the single phonon device.

Author Contributions: Conceptualization, Z.D.; formal analysis, Y.S. and B.H.; investigation, Y.R.; writing—original draft preparation, Y.R.; writing—review and editing, Z.D.; supervision, Z.D. All authors have read and agreed to the published version of the manuscript.

Funding: This study was funded by the National Natural Science Foundation of China (11964014, 11664014, and 12064018); Major Discipline Academic and Technical Leaders Training Program of Jiangxi Province (20204BCJ23026); and the Natural Science Foundation of Jiangxi Province (20212BAB201018).

Data Availability Statement: Not applicable.

Conflicts of Interest: The authors declare no conflict of interest.

Appendix A

In the weak driving limit, high phonon occupation (the phonon number is larger than 2) is extremely low. Hence, we can truncate the Hilbert space of the system and keep it up to finite space. In finite Hilbert space ($n \leq 3$), the Hamiltonian for our system can be expressed as:

$$H = \begin{pmatrix} 0 & F & \sqrt{2}\chi e^{-i\theta} & 0 \\ F & \Delta_0 & \sqrt{2}F & \sqrt{6}\chi e^{-i\theta} \\ \sqrt{2}\chi e^{i\theta} & \sqrt{2}F & 2\Delta_0 & \sqrt{3}F \\ 0 & \sqrt{6}\chi e^{i\theta} & \sqrt{3}F & 3\Delta_0 \end{pmatrix}. \tag{A1}$$

The corresponding density matrix is:

$$\rho = \begin{pmatrix} \rho_{00} & \rho_{01} & \rho_{02} & \rho_{03} \\ \rho_{10} & \rho_{11} & \rho_{12} & \rho_{13} \\ \rho_{20} & \rho_{21} & \rho_{22} & \rho_{23} \\ \rho_{30} & \rho_{31} & \rho_{32} & \rho_{33} \end{pmatrix}. \tag{A2}$$

Substituting the Hamiltonian (A1) and the density matrix (A2) into the steady-state master equation $L\hat{\rho} = 0$, after straightforward calculation, we obtain the following coupled equations for the density matrix elements

$$0 = i\kappa\rho_{11} + \sqrt{2}(\chi e^{-i\theta}\rho_{20} - \chi e^{i\theta}\rho_{02}) + F(\rho_{10} - \rho_{01}) + i\kappa\bar{n}(\rho_{11} - \rho_{00}), \tag{A3}$$

$$0 = \left(\Delta_0 - \frac{1}{2}i\kappa\right)\rho_{10} + \sqrt{6}\chi e^{-i\theta}\rho_{30} - \sqrt{2}\chi e^{i\theta}\rho_{12} + \sqrt{2}i\kappa\rho_{21} + F(\rho_{00} - \rho_{11}) + \sqrt{2}F\rho_{20} + \sqrt{2}i\kappa\bar{n}(\rho_{21} - \sqrt{2}\rho_{10}), \tag{A4}$$

$$0 = 2\left(\Delta_0 - \frac{1}{2}i\kappa\right)\rho_{20} + \sqrt{2}\chi e^{i\theta}(\rho_{00} - \rho_{22}) - F\rho_{21} + \sqrt{3}F\rho_{30} + \sqrt{2}F\rho_{10} + \sqrt{3}i\kappa\rho_{31} + \sqrt{3}i\kappa\bar{n}(\rho_{31} - \sqrt{3}\rho_{20}), \tag{A5}$$

$$0 = 3\left(\Delta_0 - \frac{1}{2}i\kappa\right)\rho_{30} + \sqrt{2}\chi e^{i\theta}(\sqrt{3}\rho_{10} - \rho_{32}) + \sqrt{3}F\rho_{20} - F\rho_{31} - 4i\kappa\bar{n}\rho_{30}, \tag{A6}$$

$$\begin{aligned}
 0 = & \quad i\kappa(2\rho_{22} - \rho_{11}) + \sqrt{6}(\chi e^{-i\theta}\rho_{31} - \chi e^{i\theta}\rho_{13}) \\
 & + \sqrt{2}F(\rho_{21} - \rho_{12}) + F(\rho_{01} - \rho_{10}) \\
 & + i\kappa\bar{n}(\rho_{00} - 3\rho_{11} + 2\rho_{22}),
 \end{aligned} \tag{A7}$$

$$\begin{aligned}
 0 = & \quad \left(\Delta_0 - \frac{3}{2}i\kappa\right)\rho_{21} + \sqrt{2}\chi e^{i\theta}(\rho_{01} - \sqrt{3}\rho_{23}) \\
 & + \sqrt{2}F(\rho_{11} - \rho_{22}) - F\rho_{20} + \sqrt{3}F\rho_{31} \\
 & + \sqrt{6}i\kappa\rho_{32} + i\kappa\bar{n}(\sqrt{2}\rho_{10} - 4\rho_{21} + \sqrt{6}\rho_{32}),
 \end{aligned} \tag{A8}$$

$$\begin{aligned}
 0 = & \quad 2(\Delta_0 - i\kappa)\rho_{31} + \sqrt{6}\chi e^{i\theta}(\rho_{11} - \rho_{33}) \\
 & + F(\sqrt{3}\rho_{21} - \rho_{30} - \sqrt{2}\rho_{32}) \\
 & + i\kappa\bar{n}(\sqrt{3}\rho_{20} - 5\rho_{31}),
 \end{aligned} \tag{A9}$$

$$\begin{aligned}
 0 = & \quad i\kappa(3\rho_{33} - 2\rho_{22}) + \sqrt{2}\chi(e^{-i\theta}\rho_{20} - e^{i\theta}\rho_{02}) \\
 & + \sqrt{2}F(\rho_{21} - \rho_{12}) + \sqrt{3}F(\rho_{32} - \rho_{23}) \\
 & - i\kappa\bar{n}(2\rho_{11} + 5\rho_{22} - 3\rho_{33}),
 \end{aligned} \tag{A10}$$

$$\begin{aligned}
 0 = & \quad \left(\Delta_0 - \frac{5}{2}i\kappa\right)\rho_{32} + \sqrt{6}\chi e^{i\theta}\rho_{12} - \sqrt{2}\chi e^{-i\theta}\rho_{30} \\
 & - \sqrt{2}F\rho_{31} + \sqrt{3}F(\rho_{22} - \rho_{33}) \\
 & + \sqrt{6}i\kappa\bar{n}(\rho_{21} - \sqrt{6}\rho_{32}),
 \end{aligned} \tag{A11}$$

$$\begin{aligned}
 0 = & \quad -3i\kappa\rho_{33} + \sqrt{6}\chi(e^{i\theta}\rho_{13} - e^{-i\theta}\rho_{31}) \\
 & + \sqrt{3}F(\rho_{23} - \rho_{32}) + i\kappa\bar{n}(3\rho_{22} - 7\rho_{33}),
 \end{aligned} \tag{A12}$$

Under the assumption of a weak driving limit and low temperature limit, $\rho_{00} \simeq 1$, $\rho_{00} \gg \rho_{11} \gg \rho_{22}$, $1 \gg n_{th}$, we obtain the matrix elements by iteration

$$\rho_{10} = \frac{-\Delta^*F}{(1 + 2\bar{n})|\Delta|^2 + 2F^2}, \tag{A13}$$

$$\rho_{11} = \frac{\bar{n}|\Delta|^2 + F^2}{(1 + 2\bar{n})|\Delta|^2 + 2F^2}, \tag{A14}$$

$$\rho_{20} = \sqrt{2} \frac{(F^2 - \Delta\chi e^{i\theta}) - (2F^2 - \Delta\chi e^{i\theta})\rho_{11}}{\Delta^2}, \tag{A15}$$

$$\begin{aligned}
 \rho_{21} = & \quad \frac{2\sqrt{2}}{\Delta}F\bar{n}^2 + \frac{3F^2 + \Delta\chi e^{i\theta} - 2|\Delta|^2}{\sqrt{2}\Delta|\Delta|^2}F\bar{n} \\
 & + \frac{F^2(2\Delta\chi e^{i\theta} + \Delta^*\chi e^{-i\theta}) - 3|\Delta|^2\chi^2}{\sqrt{2}\Delta|\Delta|^4}F \\
 & - \frac{(F^2 - \Delta\chi e^{i\theta})}{\sqrt{2}\Delta|\Delta|^2}F,
 \end{aligned} \tag{A16}$$

$$\begin{aligned} \rho_{22} = & \left(1 - \frac{6F^2}{|\Delta|^2}\right) \bar{n}^2 + \frac{\chi^2 |\Delta|^2 - 3F^4 + 2F^2 |\Delta|^2}{|\Delta|^4} \bar{n} \\ & + \frac{|F^2 - \Delta \chi e^{i\theta}|^2}{|\Delta|^4} \bar{n} + \frac{3\chi^2 |\Delta|^2 - F^4}{|\Delta|^6} F^2 \\ & + \frac{(2E^2 + |\Delta|^2) |F^2 - \Delta \chi e^{i\theta}|^2}{2|\Delta|^6}, \end{aligned} \quad (\text{A17})$$

$$\rho_{30} = -\frac{(F^2 - 3\Delta \chi e^{i\theta})}{\sqrt{6}\Delta^3} F, \quad (\text{A18})$$

$$\rho_{31} = \sqrt{3} \frac{F^2 - \Delta \chi e^{i\theta}}{\sqrt{2}\Delta^2} \bar{n} + \frac{(F^2 - 3\Delta \chi e^{i\theta})}{\sqrt{6}|\Delta|^2 \Delta^2} F^2, \quad (\text{A19})$$

$$\begin{aligned} \rho_{32} = & -\frac{\sqrt{3}F}{\Delta} \bar{n}^2 + \sqrt{3}F \frac{\Delta \chi e^{i\theta} - F^2}{|\Delta|^2 \Delta} \bar{n} \\ & - \frac{(F^2 - 3\Delta \chi e^{i\theta})(F^2 - \Delta^* \chi e^{-i\theta})}{2\sqrt{3}|\Delta|^4 \Delta} F, \end{aligned} \quad (\text{A20})$$

$$\begin{aligned} \rho_{33} = & \frac{3F^2}{|\Delta|^2} \bar{n}^2 + \frac{3|F^2 - \Delta \chi e^{i\theta}|^2}{2|\Delta|^4} \bar{n} \\ & + \frac{|F^2 - 3\Delta \chi e^{i\theta}|^2 F^2}{6|\Delta|^6}. \end{aligned} \quad (\text{A21})$$

References

1. Sklan, S.R. Splash, pop, sizzle: Information processing with phononic computing. *AIP Adv.* **2015**, *5*, 053302. [[CrossRef](#)]
2. Meher, N. A proposal for the implementation of quantum gates in an optomechanical system via phonon blockade. *J. Phys. B At. Mol. Opt. Phys.* **2019**, *52*, 205502. [[CrossRef](#)]
3. Zhao, C.; Peng, R.; Yang, Z.; Chao, S.; Li, C.; Zhou, L. Atom Mediated Phonon Blockade and Controlled Z Gate in Superconducting Circuit System. *Ann. Phys.* **2021**, *533*, 2100039. [[CrossRef](#)]
4. Cardenas-Lopez, F.; Romero, G.; Lamata, L.; Solano, E.; Retamal, J. Parity-Assisted Generation of Nonclassical States of Light in Circuit Quantum Electrodynamics. *Symmetry* **2019**, *11*, 372. [[CrossRef](#)]
5. Zhang, Z.; Jiang, X.; Tang, S. Realization of Quantum Swap Gate and Generation of Entangled Coherent States. *Symmetry* **2022**, *14*, 1951. [[CrossRef](#)]
6. Liu, Y.X.; Miranowicz, A.; Gao, Y.B.; Bajer, J.; Sun, C.P.; Nori, F. Qubit-induced phonon blockade as a signature of quantum behavior in nanomechanical resonators. *Phys. Rev. A* **2010**, *82*, 032101. [[CrossRef](#)]
7. Cai, K.; Pan, Z.W.; Wang, R.X.; Ruan, D.; Yin, Z.Q.; Long, G.L. Single phonon source based on a giant polariton nonlinear effect. *Opt. Lett.* **2018**, *43*, 1163–1166. [[CrossRef](#)]
8. Miranowicz, A.; Bajer, J.; Lambert, N.; Liu, Y.X.; Nori, F. Tunable multiphonon blockade in coupled nanomechanical resonators. *Phys. Rev. A* **2016**, *93*, 013808. [[CrossRef](#)]
9. Xu, X.W.; Chen, A.X.; Liu, Y.X. Phonon blockade in a nanomechanical resonator resonantly coupled to a qubit. *Phys. Rev. A* **2016**, *94*, 063853. [[CrossRef](#)]
10. Didier, N.; Pugnetti, S.; Blanter, Y.M.; Fazio, R. Detecting phonon blockade with photons. *Phys. Rev. B* **2011**, *84*, 054503. [[CrossRef](#)]
11. Ramos, T.; Sudhir, V.; Stannigel, K.; Zoller, P.; Kippenberg, T.J. Nonlinear quantum optomechanics via individual intrinsic two-level defects. *Phys. Rev. Lett.* **2013**, *110*, 193602. [[CrossRef](#)] [[PubMed](#)]
12. Wang, X.; Miranowicz, A.; Li, H.R.; Nori, F. Method for observing robust and tunable phonon blockade in a nanomechanical resonator coupled to a charge qubit. *Phys. Rev. A* **2016**, *93*, 063861. [[CrossRef](#)]
13. Guan, S.; Bowen, W.P.; Liu, C.; Duan, Z. Phonon antibunching effect in coupled nonlinear micro/nanomechanical resonator at finite temperature. *EPL* **2017**, *119*, 58001. [[CrossRef](#)]
14. Sarma, B.; Sarma, A.K. Tunable phonon blockade in weakly nonlinear coupled mechanical resonators via Coulomb interaction. *Sci. Rep.* **2018**, *8*, 14583. [[CrossRef](#)]
15. Shi, H.Q.; Zhou, X.T.; Xu, X.W.; Liu, N.H. Tunable phonon blockade in quadratically coupled optomechanical systems. *Sci. Rep.* **2018**, *8*, 2212. [[CrossRef](#)]

16. Shi, H.Q.; Xie, Z.Q.; Xu, X.W.; Liu, N.H. Unconventional phonon blockade in multimode optomechanical system. *Acta Phys. Sin.* **2018**, *67*, 044203. [[CrossRef](#)]
17. Yang, J.-Y.; Jin, Z.; Liu, J.-S.; Wang, H.-F.; Zhu, A.D. Unconventional Phonon Blockade in a Tavis–Cummings Coupled Optomechanical System. *Ann. Phys.* **2020**, *532*, 2000299. [[CrossRef](#)]
18. Zhao, C.; Li, X.; Chao, S.; Peng, R.; Li, C.; Zhou, L. Simultaneous blockade of a photon, phonon, and magnon induced by a two-level atom. *Phys. Rev. A* **2020**, *101*, 063838. [[CrossRef](#)]
19. Nema, J.K.; Gupta, S.; Thakkar, R.; Rajagopal, P. Novel hermetically sealed device to realize unconventional phonon blockade at near-micron dimensions and milliKelvin temperatures. *AIP Adv.* **2021**, *11*, 015112. [[CrossRef](#)]
20. Wang, M.; Yin, T.-S.; Sun, Z.-Y.; Cheng, H.-G.; Zhan, B.-F.; Zheng, L.-L. Unconventional phonon blockade via atom-photon-phonon interaction in hybrid optomechanical systems. *Opt. Express* **2022**, *30*, 10251–10268. [[CrossRef](#)]
21. Zeng, Y.X.; Gebremariam, T.; Shen, J.; Xiong, B.; Li, C. Application of machine learning for predicting strong phonon blockade. *Appl. Phys. Lett.* **2021**, *118*, 164003. [[CrossRef](#)]
22. Restrepo, J.; Favero, I.; Ciuti, C. Fully coupled hybrid cavity optomechanics: Quantum interferences and correlations. *Phys. Rev. A* **2017**, *95*, 023832. [[CrossRef](#)]
23. Xie, H.; Liao, C.-G.; Shang, X.; Ye, M.Y.; Lin, X.M. Phonon blockade in a quadratically coupled optomechanical system. *Phys. Rev. A* **2017**, *96*, 013861. [[CrossRef](#)]
24. Xu, X.-W.; Shi, H.-Q.; Chen, A.-X.; Liu, Y.-X. Cross-correlation between photons and phonons in quadratically coupled optomechanical systems. *Phys. Rev. A* **2018**, *98*, 013821. [[CrossRef](#)]
25. Yao, X.-Y.; Ali, H.; Li, F.-L.; Li, P.-B. Nonreciprocal Phonon Blockade in a Spinning Acoustic Ring Cavity Coupled to a Two-Level System. *Phys. Rev. Appl.* **2022**, *17*, 054004. [[CrossRef](#)]
26. Li, Z.-Y.; Jin, G.-R.; Yin, T.-S.; Chen, A.X. Two-phonon blockade in quadratically coupled optomechanical systems. *Photonics* **2022**, *9*, 70. [[CrossRef](#)]
27. Kowalewska-Kudlaszyk, A.; Abo, S.I.; Chmiczak, G.; Perina, J.; Nori, F.; Miranowicz, A. Two-photon blockade and photon-induced tunneling generated by squeezing. *Phys. Rev. A* **2019**, *100*, 053857. [[CrossRef](#)]
28. LaHaye, M.D.; Buu, O.; Camarota, B.; Schwab, K.C. Approaching the quantum limit of a nanomechanical resonator. *Science* **2004**, *304*, 74–77. [[CrossRef](#)]
29. Schwab, K.C.; Roukes, M.L. Putting mechanics into quantum mechanics. *Phys. Today* **2005**, *58*, 36–42. [[CrossRef](#)]
30. Carmon, T.; Rokhsari, H.; Yang, L.; Kippenberg, T.J.; Vahala, K.J. Temporal behavior of radiation-pressure-induced vibrations of an optical microcavity phonon mode. *Phys. Rev. Lett.* **2005**, *94*, 223902. [[CrossRef](#)]
31. Aspelmeyer, M.; Kippenberg, T.J.; Marquardt, F. Cavity optomechanics. *Rev. Mod. Phys.* **2014**, *86*, 1391. [[CrossRef](#)]
32. Connell, A.D.; Hofheinz, M.; Ansmann, M.; Bialczak, R.C.; Lenander, M.; Lucero, E.; Neeley, M.; Sank, D.; Wang, H.; Weides, M.; Wenner, J.; Martinis, J.M.; Cleland, A.N. Quantum ground state and single-phonon control of a mechanical resonator. *Nature* **2010**, *464*, 697–703. [[CrossRef](#)] [[PubMed](#)]
33. Yan, Y.-Y.; Cheng, Y.-B.; Guan, S.-G.; Yu, D.-Y.; Duan, Z. Pulse-regulated single-photon generation via quantum interference in a $\chi^{(2)}$ nonlinear nanocavity. *Opt. Lett.* **2018**, *43*, 5086–5089. [[CrossRef](#)] [[PubMed](#)]
34. Lemonde, M.-A.; Didier, N.; Clerk, A.A. Enhanced nonlinear interactions in quantum optomechanics via mechanical amplification. *Nat. Commun.* **2016**, *7*, 11338. [[CrossRef](#)]
35. Li, P.-B.; Zhou, Y.; Gao, W.-B.; Nori, F. Enhancing spin-phonon and spin-spin interactions using linear resources in a hybrid quantum system. *Phys. Rev. Lett.* **2020**, *125*, 153602. [[CrossRef](#)]
36. Wang, Y.; Wu, J.-L.; Han, J.-X.; Xia, Y.; Jiang, Y.-Y.; Song, J. Enhanced phonon blockade in a weakly coupled hybrid system via mechanical parametric amplification. *Phys. Rev. Appl.* **2022**, *17*, 024009. [[CrossRef](#)]
37. Szorkovszky, A.; Brawley, G.A.; Doherty, A.C.; Bowen, W.P. Strong thermomechanical squeezing via weak measurement. *Phys. Rev. Lett.* **2013**, *110*, 184301. [[CrossRef](#)] [[PubMed](#)]
38. Miranowicz, A.; Bajer, J.; Paprzycka, M.; Liu, Y.-X.; Zagoskin, A.M.; Nori, F. State-dependent photon blockade via quantum-reservoir engineering. *Phys. Rev. A* **2014**, *90*, 033831. [[CrossRef](#)]
39. Kimble, H.J.; Dagenais, M.; Mandel, L. Photon antibunching in resonance fluorescence. *Phys. Rev. Lett.* **1977**, *39*, 691. [[CrossRef](#)]
40. Meiser, D.; Holland, M.J. Intensity fluctuations in steady-state superradiance. *Phys. Rev. A* **2010**, *81*, 063827. [[CrossRef](#)]
41. Gardiner, C.; Zoller, P. *Quantum Noise*; Springer: Berlin/Heidelberg, Germany, 2004.

Disclaimer/Publisher’s Note: The statements, opinions and data contained in all publications are solely those of the individual author(s) and contributor(s) and not of MDPI and/or the editor(s). MDPI and/or the editor(s) disclaim responsibility for any injury to people or property resulting from any ideas, methods, instructions or products referred to in the content.